Ascent Performance of an Air-Breathing Horizontal-Takeoff Launch Vehicle

Richard W. Powell,* John D. Shaughnessy,† Christopher I. Cruz,* and J. Christopher Naftel*
NASA Langley Research Center, Hampton, Virginia 23665

Advanced manned launch systems studies underway at the NASA Langley Research Center are part of a broad effort examination of options for the next manned space transportation system to be developed by the United States. One promising concept that uses advanced technologies is a fully reusable, single-stage horizontal-takeoff vehicle that uses airbreathing propulsion. This paper discusses some potential ascent issues that could influence the design of this class of launch vehicles. Two issues are identified. The first issue is that the drag losses due to aerodynamic trim can require a significant fraction of the total energy required to achieve orbit. The second issue is the difficulty in achieving precision insertions with a vehicle that coasts unpowered from a high dynamic pressure to orbit.

Nomenclature

A_c = engine capture area, m^2
A_s = sensed acceleration, g
C_D = drag coefficient, nondimensional, = (drag/$q_\infty S$)
C_L = lift coefficient, nondimensional, = (lift/$q_\infty S$)
C_m = pitching-moment coefficient, nondimensional, = (pitching moment/$q_\infty Sc$)
C_T = thrust coefficient, nondimensional, = (thrust/$q_\infty A_c$)
c = mean aerodynamic chord, m
h = altitude, m
I_{sp} = specific impulse, s
K_p = roll rate gain, s
K_q = pitch rate gain, s
$K_{\dot{q}}$ = pitch acceleration gain, s^2
K_r = yaw rate gain, s
K_α = angle-of-attack error gain, nondimensional
K_{α_I} = integral of angle-of-attack error gain, s^{-1}
K_β = sideslip angle gain, nondimensional
K_ϕ = roll error gain, nondimensional
p = roll rate, deg/s
q = pitch rate, deg/s
$\dot{q}$ = time derivative of dynamic pressure, Pa/s
q_c = commanded dynamic pressure, Pa
q_∞ = dynamic pressure, Pa
$q\alpha$ = product of dynamic pressure and angle of attack, Pa-deg
r = yaw rate, deg/s
S = reference area, m^2
V_I = inertial velocity, m/s
V_R = Earth relative velocity, m/s
α = angle of attack deg
α_c = commanded angle of attack, deg
α_{nom} = nominal angle of attack, deg
β = sideslip angle, deg
γ = flight-path angle, deg
γ_c = commanded flight-path angle, deg
ΔApogee = change in apogee at orbital insertion as compared with optimal trajectory, km
$\Delta C_{D_{\delta e}}$ = drag coefficient increment due to elevon deflection, nondimensional, = (drag increment/$q_\infty S$)
$\Delta C_{L_{\delta e}}$ = lift coefficient increment due to elevon deflection, nondimensional, = (lift increment/$q_\infty S$)
$\Delta C_{m_{\delta e}}$ = pitching moment coefficient increment due to elevon deflection, nondimensional, = (pitching-moment increment/$q_\infty Sc$)
ΔPayload = change in delivered payload as compared with optimal trajectory, kg
ΔPerigee = change in perigee at orbital insertion as compared with optimal trajectory, km
ΔTime = change in orbital insertion time as compared with optimal trajectory (positive longer), s
ΔV_{aero} = velocity loss increment due to aerodynamics, m/s
ΔV_{circ} = instantaneous velocity required to circularize, m/s
ΔV_{cor} = velocity loss increment due to Coriolis effect, m/s
ΔV_{grav} = velocity loss increment due to gravity, m/s
ΔV_{ideal} = ideal velocity increment, m/s
ΔV_{loss} = total velocity loss increments, m/s
ΔV_{thrust} = velocity loss increment due to reduced thrust induced by atmospheric pressure, m/s
ΔV_{tv} = velocity loss increment due to thrust vector misalignments, m/s
δa = aileron deflection, = [($\delta e_l - \delta e_r$)/2)], deg
δa_c = commanded aileron deflection, deg
δe = elevator deflection, = [($\delta e_l + \delta e_r$)/2)], deg
δe_c = commanded elevation deflection, deg
δe_i = initial elevator deflection, deg
δe_l = left elevon deflection (positive trailing-edge down), deg
δe_r = right elevon deflection (positive trailing edge down), deg
δ_r = rudder deflection (positive trailing-edge left), deg
δr_c = commanded rudder deflection, deg
ρ = atmospheric density, kg/m^3
ρ_{76} = 1976 standard atmospheric density, kg/m^3
ϕ = roll angle, deg
ϕ_c = commanded roll angle, deg
σ = atmospheric density standard deviation as calculated by global reference atmosphere model, nondimensional

Received Feb. 28, 1990; revision received July 6, 1990; accepted for publication Aug. 2, 1990.

*Aerospace Engineer, Space Systems Division, Mail Stop 365. Member AIAA.
†Aerospace Engineer, Guidance and Control Division, Mail Stop 489. Member AIAA.

Introduction

EARTH-to-orbit space transportation concepts have been studied for many year to fulfill a variety of anticipated mission needs.[1-4] The primary objectives have been to define vehicles that both substantially reduce the cost of manned space transportation and provide a complement to a transportation architecture to support a wide range of scientific, military, and commercial uses. These studies have identified concepts using both near-term and more advanced technology. One of the promising concepts using advanced technology is a fully reusable, single-stage vehicle with air-breathing propulsion. Because a vehicle of this class has never flown, an analysis of the ascent, including six-degree-of-freedom simulations, was conducted to determine if any problems that may influence the design of such a vehicle would be uncovered.

This paper discusses the optimal ascent flight profile for this vehicle, the design of the guidance and control algorithms, the issues related to trim drag, the description of the off-nominal conditions used in the simulations, and the result of simulations with these off-nominal conditions.

Vehicle Description

The vehicle used for this study employs all-airbreathing propulsion from takeoff to orbit insertion. Figure 1 shows this concept and Table 1 shows its major characteristics. This vehicle is composed of an axisymmetric 5-deg half-angle conical forebody, a cylindrical engine nacelle section, and a cone frustrum nozzle. The wing has a leading-edge sweep of 78 deg and is set at 0-deg incidence and dihedral. The wing is a 4% thick diamond airfoil. Elevons are located at the trailing edge of the wing with their hinge line perpendicular to the fuselage centerline. The vertical tail is a 4% thick diamond airfoil with a leading-edge sweep angle of 70 deg and includes a rudder with a hinge line at the 75% chord position measured from the leading edge. The canards have a 6% thick symmetrical 65A series airfoil, are deployed only at subsonic speeds, and are kept at 0-deg incidence relative to the fuelage centerline.

Aerodynamics Model

The aerodynamic data base for this vehicle was generated using the Aerodynamic Preliminary Analysis System (APAS).[5,6] APAS is an interactive computer code that predicts the aerodynamic characteristics of a vehicle from subsonic to hypersonic speeds using a common geometric definition. APAS incorporates a variety of engineering techniques to estimate the basic longitudinal and lateral-directional characteristics of vehicles as well as control effectiveness and dynamic derivatives. The data used for this vehicle can be found in Ref. 7.

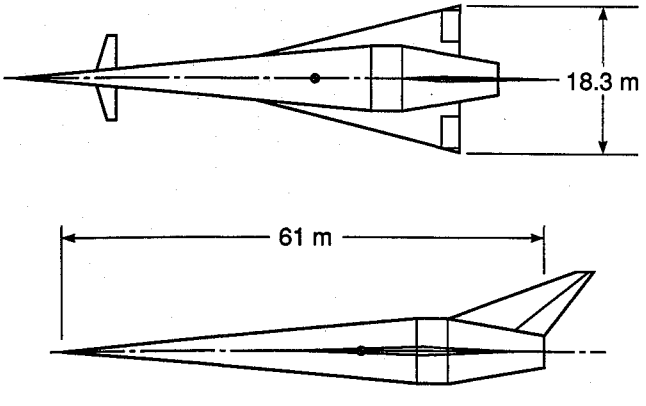

Fig. 1 Horizontal-takeoff air-breathing vehicle.

Table 1 Vehicle characteristics

Gross mass, kg	136,079
Dry mass, kg	58,968
Payload, kg	9,100
Circularization engine I_{sp}, s	465
Wing reference area, m^2	335
Span, m	18
Mean aerodynamic chord, m	24

Propulsion Model

The propulsion model used in the study was created by using a modified version of a cycle analysis method described in Ref. 8. The thrust coefficient and specific impulse were determined as functions of Mach number, dynamic pressure, and fuel equivalence ratio and are presented in Ref. 7. The specific impulse and thrust coefficient characteristics for the propulsion system for the nominal dynamic pressure and fuel equivalence ratio are shown in Figs. 2 and 3.

Mass Model

The vehicle mass model is based on the assumption of a rigid structure and distributed fuel. Fuel slosh is not considered. The mass, moments of inertia, and the center-of-gravity (c.g.) location of the vehicle are modeled a functions of the remaining onboard propellant. The products of inertia are neglected. The weight of fuel consumed is obtained by integrating the fuel flow rate over the time the engines are thrusting. More detail of the mass model used can be found in Ref. 7.

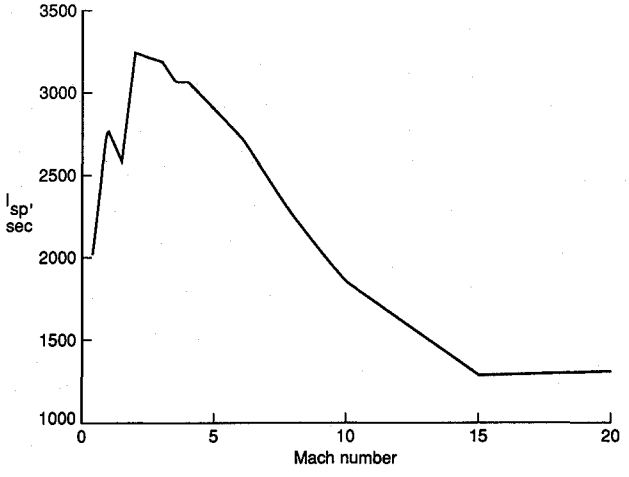

Fig. 2 Air-breathing engine specific impulse characteristics.

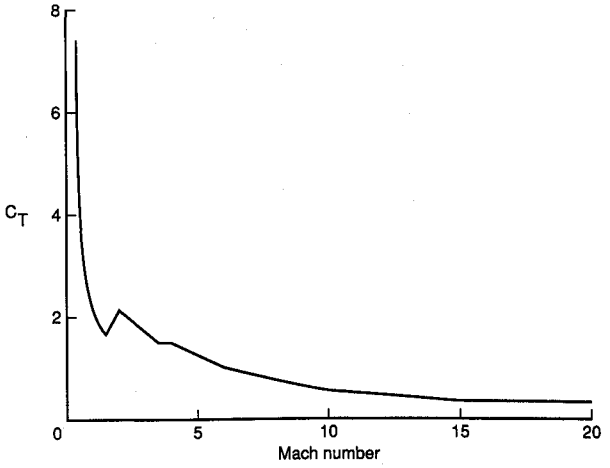

Fig. 3 Air-breathing engine thrust coefficients characteristics.

Atmospheric Profile Modeling

Off-nominal atmospheric conditions, both density and wind profiles, were used as part of the six-degree-of-freedom simulations. The first off-nominal conditions used were constant bias factors between 0.8 and 1.2 applied to the standard atmospheric density which for these studies is the U.S. Standard Atmosphere, 1976.[9] To simulate a more realistic variation in atmospheric density, density profiles were generated using the Global Reference Atmosphere Model (GRAM).[10] The GRAM was developed to provide realistic worldwide atmospheric data including winds. The GRAM can be used to generate the monthly mean and perturbation data. A total of 41 simulations were generated. These are as follows: 1) nominal 1976 atmosphere with no winds, 2) factors of 0.8, 0.9, 1.1, and 1.2 applied to nominal 1976 atmosphere with no winds, 3) monthly mean data with no winds, 4) monthly mean data with winds, 5) 10 perturbed atmospheres with winds for selected date (July 1, 1989), and 6) 3σ data for selected date (July 1, 1989). Figures 4–6 show the range of atmospheric density and wind profiles generated by GRAM and used in this study.

Trajectory Simulations

All of the trajectories presented in this paper were generated by either the three-degree-of-freedom or the six-degree-of-freedom version of the Program to Optimize Simulated Trajectories (POST).[11] POST is a generalized event-oriented trajectory program that can be used to analyze ascent, on-orbit, and entry trajectories. POST can be used to optimize any calculated variable that may be subjected to a combination of both equality and inequality constraint.

The POST program has been modified to include a predictor-corrector guidance capability. The predictor-corrector capability was implemented by including a three-degree-of-freedom simulation as an inner loop to the main simulation. This allows the predictor-corrector guidance model to have different environmental characteristics (planet, atmosphere, gravity, aerodynamic, propulsion, weights, etc.) than the main simulation. For this study, identical models, with the exception of the atmosphere, were used by both the main simulation and the predictor-corrector guidance algorithm. The predictor-corrector guidance models used the U.S. Standard Atmosphere, 1976 that was modified, as discussed later. The predictor-corrector models did not include winds.

In general, the predictor-corrector algorithm determines a set of controls that will meet a specified set of constraints within specified tolerances. This is done by numerically integrating the three-degree-of-freedom (translation modes) equations from within the guidance loop of the simulation. Because of the importance of lift and drag increments due to control deflections, these equations have been modified to include these effects by determining the elevator deflections required to statically trim the vehicle in pitch. Once the predictor-corrector algorithm is activated, it integrates the equations of motion until the specified termination condition using the nominal values of controls. These nominal values are initially a user-supplied estimate, but they are updated after each iteration. At this time, the equations are integrated once for each control to determine numerical sensitivities using a forward differencing technique. Each control is modified individually. Then, assuming the derivatives are linear with no cross dependencies, the controls are modified using a Newton-Raphson technique. This process is repeated until all constraints are within specified tolerances. This technique requires that the number of constants be equal to the number of controls. Because the linearity assumption is only valid over some limited range, the amount each control is allowed to change for each iteration is limited. The set of controls that meet the constraints is then provided to the guidance algorithm for implementation. The predictor-corrector algorithm is called at user-specified time increments.

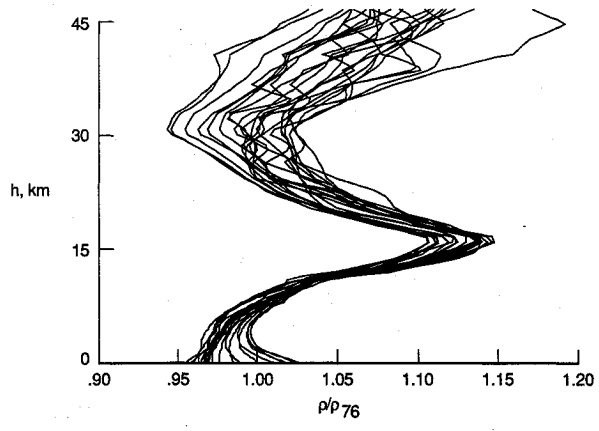

Fig. 4 Atmospheric density profiles calculated by GRAM.

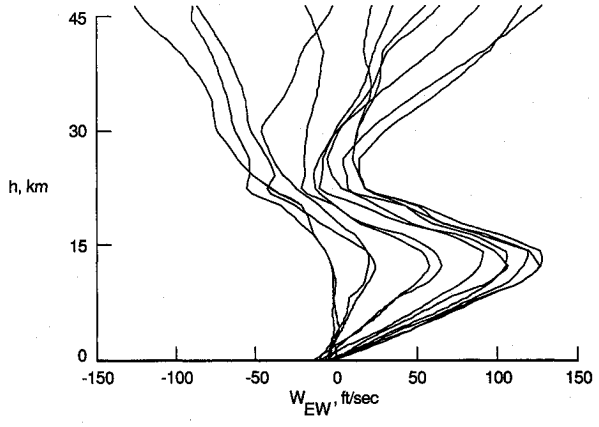

Fig. 5 East-west wind components calculated by GRAM.

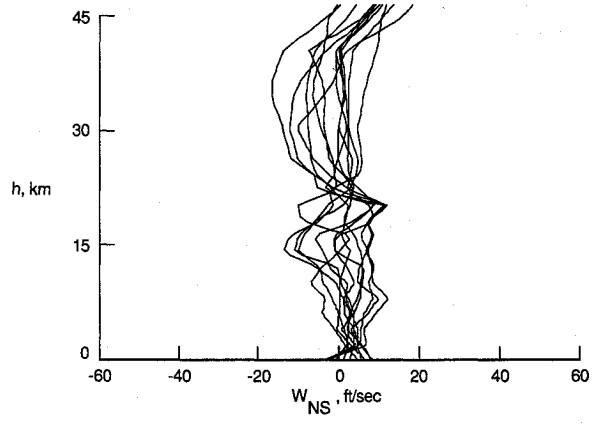

Fig. 6 North-south wind components calculated by GRAM.

Design Trajectory

The design trajectory was a due east launch from the NASA Kennedy Space Center that circularized at 185 km. This trajectory was designed to maximize inserted payload without violating any vehicle design constraints. The most significant constraint was a dynamic pressure limit of 60 kPa for velocities less than Mach 1 and a limit of 95 kPa for velocities greater than Mach 3. Between Mach 1 and Mach 3, the dynamic pressure constraint was varied linearly between these limits. The optimal trajectory, as determined by the three-degree-of-freedom verion of POST, dictated that the vehicle reach the 95-kPa limit as quickly as possible and fly this boundary until sufficient velocity was obtained so that the vehicle could pull up to a transfer orbit. At this velocity, the ve-

hicle performed a powered pull up until dynamic pressure was reduced to 24 kPa. At this point, the engines were shut down and the vehicle coasted to apogee and then circularized with rocket propulsion. Time histories of this ascent are shown in Figs. 7a–c.

Guidance Algorithm

The guidance algorithm was designed to follow the optimal profile with the predictor-corrector al gorithm operating as an outer-loop control to determine the pull-up velocity. A schematic of the inner loop of the guidance algorithm is shown in Fig. 8. Much of this guidance algorithm is derived from the optimal profile discussed earlier. This includes functional relations of angle of attack α_{nom}, dynamic pressure q_c, and flight-path angle γ_c. Error signals formed by the difference of the actual state variables of dynamic pressure q_∞ and flight path angle γ, with the optimal values, namely q_c and γ_c, were added to α_{nom}. This signal was modified by the current time derivative of dynamic pressure $\dot{q}$. This type of technique involving many state variables was needed primarily to guide the vehicle from takeoff to the initial dynamic pressure boundary of 60 kPa. The wide variation in atmospheric densities (see Fig. 4) and winds (see Fig. 5) coupled with the difficulty of capturing the desired dynamic pressure profile dictated this type of guidance algorithm. Once the velocity to begin pull up is achieved, the vehicle is commanded to fly a constant angle of attack of 2 deg. The optimal trajectory shown in Figs. 7 was calculated by determining the optimal γ profile for the pull-up maneuver. However, it was found that this simplified pull-up maneuver agreed closely with the optimal maneuver. Once the engines were shut down, the vehicle was commanded to fly a minimum drag profile until apogee was reached.

The predictor corrector was initiated when velocity had reached 6 km/s and was called at 20-s time intervals afterward. The predictor corrector determined the pull-up velocity. Once the vehicle reached the velocity predicted by the algorithm, the vehicle was commanded to fly a 2-deg angle of attack α_c and maintained this angle of attack unit engine shutdown. The engines were shut down once the vehicle was predicted to be on the transfer orbit that would achieve the desired apogee. Once the engines were shut down, α_c was commanded to be 0 deg, which is the minimum drag orientation for this vehicle. The implications of this open-loop coast period will be discussed later.

The predictor-corrector algorithm used three-degree-of-freedom equations of motion that were modified to include longitudinal static aim by using elevon deflections. The aerodynamic model was composed of the untrimmed C_L, C_D, and C_m coefficients as well as $\Delta C_{L_{\delta e}}$, $\Delta C_{D_{\delta e}}$, and $\Delta C_{m_{\delta e}}$, which describe the elevator effectiveness. These aerodynamic data were derived from the aerodynamic data used in the six-degree-of-freedom simulation. The basic atmospheric model used in the predictor-corrector algorithm was the 1976 standard. However, the density profile predicted by this model had to be modified. If the atmospheric model of the predictor-corrector guidance was strictly a 1976 standard, the predictor-corrector equations of motion would see an immediate unrealistic dynamic pressure error. To correct this defect, the atmospheric density profile used by the predictor-corrector algorithm is the 1976 standard atmosphere multiplied by a constant factor, which is the ratio of the actual dynamic pressure to the dynamic pressure predicted by 1976 standard atmosphere. This factor is calculated whenever the predictor-corrector algorithm is invoked.

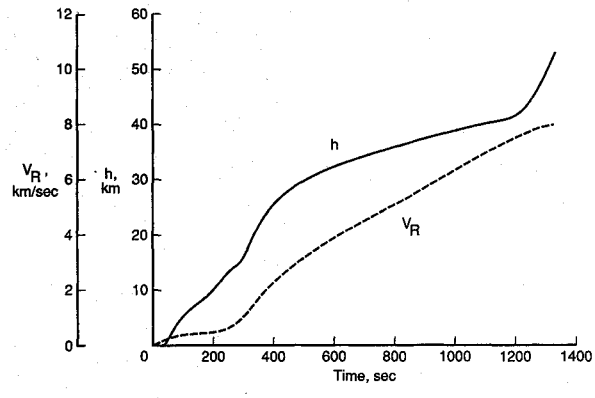

a) Altitude and velocity histories

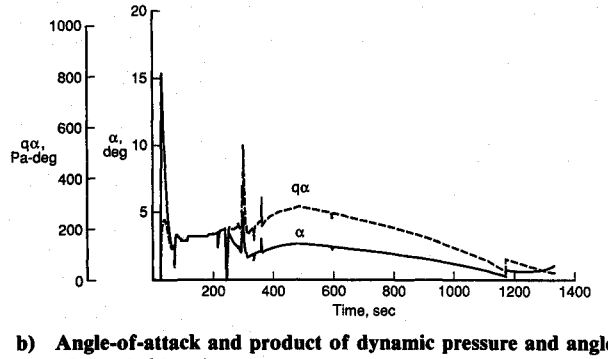

b) Angle-of-attack and product of dynamic pressure and angle-of-attack histories

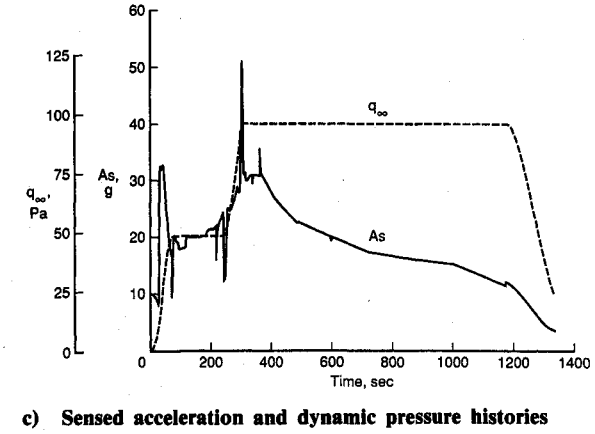

c) Sensed acceleration and dynamic pressure histories

Fig. 7 Powered ascent segment of optimal trajectory.

Flight Control System

The extensive flight time at high dynamic pressures and the use of aerodynamic control surfaces requires a six-degree-of-freedom simulation to determine accurately the flight control

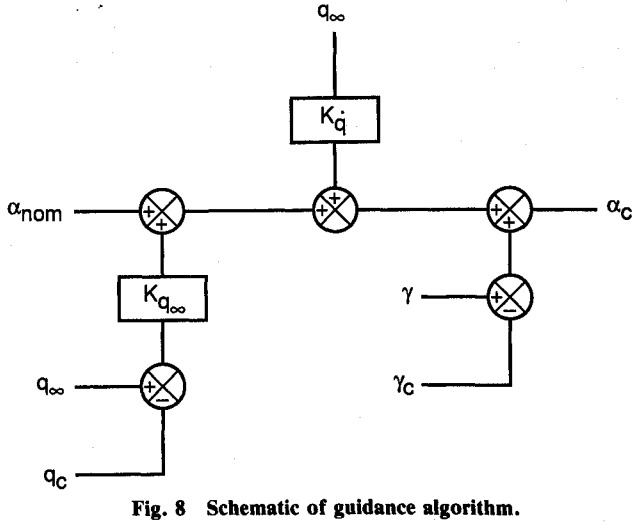

Fig. 8 Schematic of guidance algorithm.

issues. A schematic of the control system for this vehicle is shown in Fig. 9. The control philosophy was to use the elevons for both pitch and roll control. This was accomplished by differentially deflecting the elevons so that they would function both as elevators δe and ailerons δa. Thus, the elevons were used to control both angle of attack and bank angle. The elevator command was formed by an angle-of-attack error signal with pitch rate used for damping. The angle-of-attack error was formed by differencing the commanded angle of attack from the guidance algorithm with the actual angle of attack. The aileron command was formed by a roll angle error and used roll rate for damping. The roll error was formed by differencing the commanded roll angle from the guidance algorithim with the actual roll angle. For these cases, the commanded roll angle was always 0 deg. The rudder was used to control sideslip angle by using sideslip angle and yaw rate feedback. The feedback gains were determined by using a pole placement algorithm with the linear models derived from the nonlinear simulation of the vehicle. These simulations assumed perfect navigation, i.e., no error in the sensed quantities (angle of attack, roll angle, sideslip angle, pitch rate, roll rate, and yaw rate). In addition, no actuator dynamics were modeled. The engines were throttled to maintain the optimal acceleration profile, as determined by the three-degree-of-freedom analysis using POST. The engines were not gimballed for this study.

Guidance Simulations Results

The strategy that was used to assess the flight control issues was to use off-nominal atmospheric density profiles and winds. The first off-nominal conditions used in the flight control sensitivity analysis were constant bias factors applied to the standard atmospheric density. The off-nominal densities were simulated by applying factors of 0.8 – 1.2 to the standard density. The results of these cases are shown in Table 2. The results of the simulations that used the GRAM generated atmospheres are shown in Table 3. Simulations were also conducted with these same GRAM atmospheric density profiles with winds added. The results of these simulations are shown in Table 4. In addition, trajectories were simulated using 10 perturbed profiles for a single date (July 1, 1989). The results of these simulations and those with a $\pm 3\ \sigma$ variation in the mean density for this same date are shown in Table 5. The range of inserted payload for all of these cases ranged from –381 to 611 kg as compared with the nominal.

Table 2 Simulation results for constant factor atmospheric variations

	Factor = 0.8	Factor = 0.9	Factor = 1.1	Factor = 1.2
ΔPayload, kg	–381	–176	150	159
ΔTime, s	15.5	7.0	–5.9	–6.9
ΔApogee, km	0.5	0.1	0	0
ΔPerigee, km	7.8	3.6	–3.2	–6.9

Control Simulation Results

Examination of the optimal ascent illustrates some potential flight control issue that is presented in Table 6. This table lists the ideal velocities and associated velocity losses for the air-breathing vehicle used in this study. This table shows that the

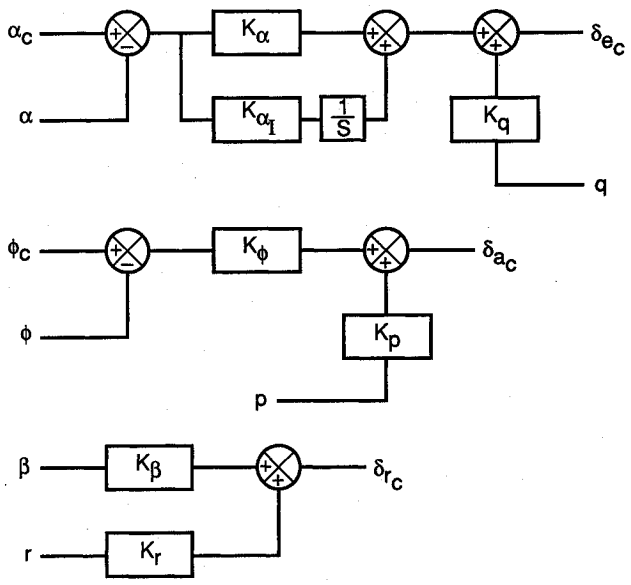

Fig. 9 Schematic of flight control system.

Table 3 Simulation results for GRAM atmospheric density variations

	January	February	March	April	May	June	July	August	September	October	November	December
ΔPayload, kg	307	249	270	475	581	557	485	341	295	239	38	290
ΔTime, s	–8.5	–6.8	–5.2	6.2	–9.7	–9.0	–7.5	–7.6	–6.3	–6.0	–7.4	–7.1
ΔApogee, km	4.9	3.6	2.0	2.6	4.2	3.0	2.0	1.6	0.9	1.6	2.8	3.2
ΔPerigee, km	–7.4	–6.0	–4.3	–4.3	7.4	–5.6	–4.8	–5.8	–4.8	–4.8	–7.2	–6.1

Table 4 Simulation results for gram atmospheric density variations (monthly mean density with winds)

	January	February	March	April	May	June	July	August	September	October	November	December
ΔPayload, kg	318	254	250	485	546	611	482	369	220	226	53	337
ΔTime, s	–7.1	–5.8	–5.2	–6.5	–10.0	–10.3	–10.3	–8.9	–6.8	–8.6	–10.3	–9.2
ΔApogee, km	5.0	4.0	2.5	3.0	4.0	3.7	3.0	2.2	3.3	2.6	3.9	4.2
ΔPerigee, km	–6.5	–4.3	–2.7	–3.2	–8.7	–3.3	–2.4	–3.9	–5.8	–2.3	–4.1	–3.0

Table 5 Simulation results for GRAM atmospheric density variations (perturbations for July 1, 1989, with winds)

	PERT 1	PERT 2	PERT 3	PERT 4	PERT 5	PERT 6	PERT 7	PERT 8	PERT 9	PERT 10	+3-σPERT	–3-σ PERT
ΔPayload, kg	487	504	508	522	507	505	452	473	509	546	583	406
ΔTime, s	–9.1	–11.4	–9.0	–11.9	–9.6	–6.8	–12.0	–9.5	–8.9	–11.3	–19.1	–0.2
ΔApogee, km	2.1	2.7	2.2	3.0	2.5	1.7	3.7	2.7	2.6	1.5	4.4	1.3
ΔPerigee, km	1.2	–3.2	0.4	–5.0	–1.6	3.2	–6.0	–1.2	–0.1	0.6	–12.6	9.4

Table 6
Ascent velocity losses

ΔV_{ideal}, m/s	10,749
ΔV_{loss}, m/s	3,372
ΔV_{aero}, m/s	2,725
ΔV_{grav}, m/s	636
ΔV_{thrust}, m/s	16
ΔV_{cor}, m/s	−5
ΔV_{circ}, m/s	162
Velocity losses due to elevon deflection, m/s	366

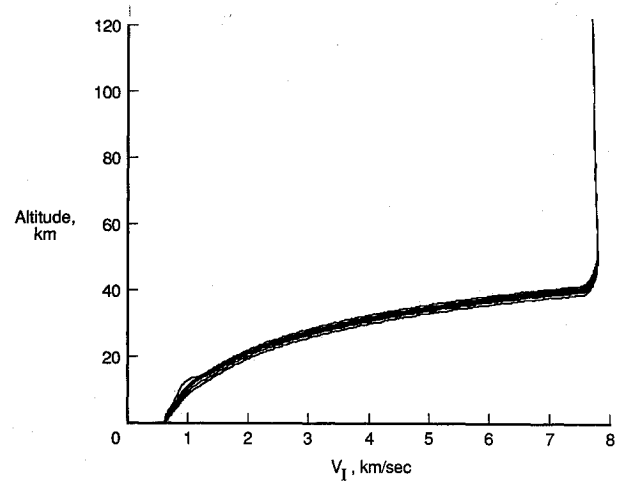

Fig. 10 Altitude velocity histories for all trajectories simulated.

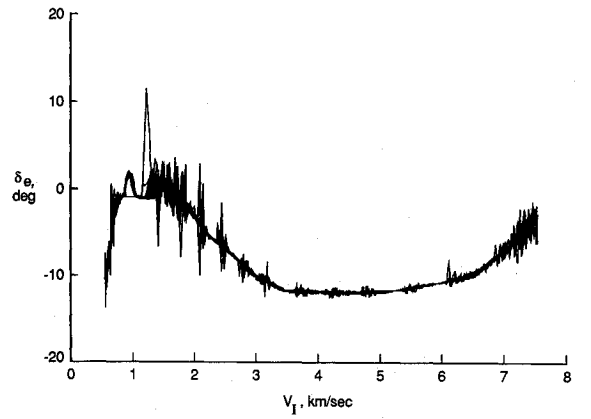

Fig. 11 Elevator deflection histories for all trajectories simulated.

velocity loss due to aim drag is 366 m/s. This large velocity loss for trim demonstrates the value of optimal c.g. control for vehicles that fly at high dynamic pressures for extended periods.

A study of trim drag reduction concepts for the present study configuration has shown that the aerodynamic center migrates forward a significant fraction of fuselage length as the flight Mach number increases to orbital values.[12] This migration causes severe aerodynamic instability and large changes in longitudinal aim moments. Use of elevons to stabilize the vehicle and counteract the aim moments results in moderate elevon deflections and excessive fuel consumption. Controlling the c.g. location so that it tracks the vehicle aerodynamic center reduces the instability and trim moment requirements, reduces elevon deflections, and results in significant fuel savings. Controlling the direction of the thrust vector to produce low-drag aim moments decreases elevon deflections and results in significant fuel savings. It was concluded that combining active c.g. position control to improve stability and minimize aim moment requirements and thrust vectoring control to generate low-drag aim moments has the potential to minimize aim drag and significantly reduce the ascent fuel consumption for horizontal takeoff vehicles. The present findings corroborate the conclusions of Ref. 12.

Guidance and Control Simulations Summary

Figure 10 shows the altitude history and Fig. 11 shows the elevator histories for all of the cases simulated. The variation in the altitude histories results from the different atmospheric density profiles, and the difference in the elevator histories results from the winds. The addition of off-nominal atmospheric conditions did not uncover additional significant issues. However, when one examines the insertion accuracy of this vehicle (Tables 2–5), one notes that this vehicle had insertion errors as high as 4.8 km. This insertion inaccuracy can be traced to the off-nominal density profiles during the open-loop coast regime. In order to improve this accuracy, the air breathing vehicle would require modulation of its drag or thrusting of the orbital maneuver engines after the main engines are shut down (24 kPa to insertion). The required change to the guidance algorithm would be minor, but more fuel would then be required for ascent. Unless rapid rendezvous is a requirement, the more fuel efficient method to correct this error would be to to include an orbital adjustment burn at perigee.

Conclusions

A study has been conducted that investigated some of the issues that affect the flight control and guidance system designs for a single-stage-to-orbit, horizontal-take off vehicle that uses air breathing propulsion until orbital insertion. Two issues were identified for this vehicle. The first was that because the aim drag losses are a significant fraction of the total ideal velocity required, the location of the center of gravity and thrust vector angle can significantly effect the amount of ascent propellant required. The second issue is that the uncertainty in the atmospheric density profile during the unpowered coast from engine shutdown to apogee results in errors in apogee as high as 4.8 km. However, this error is corrected easily once on orbit and only presents a problem if rapid rendezvous is required. If this is a requirement, drag modulation or thrusting will be required during the coast phase.

References

[1]Freeman, D. C. et al., "The Future Space Transportation System (FSTS) Study," *Astronautics & Aeronautics,* Vol. 21, No. 6, 1983, pp. 36–57.

[2]Talay, T. A., and Morris, W. D., "Advanced Manned Launch Systems," European Aerospace Conference, Paper '89-17, May 1989.

[3]Piland, W. M., and Talay, T. A., "Advanced Manned Launch Systems Comparisons," International Astronautical Federation, Paper 89-121, Oct. 1989.

[4]Martin, J. A. et al., "Orbit on Demand: In This Century If Pushed," *Astronautics & Aeronautics,* Vol. 23, No. 2, 1985, pp. 46–61.

[5]Divan, P., "Aerodynamic Preliminary Analysis System II, Part II—User's Manual," NASA CR-165628, April 1981.

[6]Cruz, C., and Wilhite A., "Prediction of High Speed Aerodynamic Characteristics Using the Aerodynamic Preliminary Analysis System," AIAA Paper 89-2173, Aug. 1989.

[7]Shaughnessy, J. D., Pinckney, S. Z., McMinn, J. D., Cruz, C. I., and Kelley, M.-L., "Hypersonic Vehicle Simulation Model: Winged-Cone Configuration," NASA TM-102610, June 1990.

[8]Pinckney, S. Z., "Internal Performance Predictions for Langley Scramjet Engine Module," NASA TM X-74038, Jan. 1978.

[9]Anon., *U.S. Standard Atmosphere, 1976,* National Oceanic and Atmospheric Administration, NASA and United States Air Force, Washington, DC, Oct. 1976.

[10]Justus, C. G., Fletcher, G. R., Gramlina, F. E., and Pace, W. B., "The NASA/MSFC Global Reference Atmospheric Model—Mod 3 (With Spherical Harmonic Wind Model)," NASA CR 3256, 1980.

[11]Brauer, G. L., Cornick, D. E., and Stevenson, R., "Capabilities and Applications of the Program to Optimize Simulated Trajectories (POST)," NASA CR-2770, Feb. 1977.

[12]Shaughnessy, J. D., "Trim Drag Reduction Concepts for Horizontal-Takeoff Single-Stage-to-Orbit Vehicles," NASA TM-102687, June 1990.